European Journal of Medicinal Chemistry 84 (2014) 628–638

Contents lists available at ScienceDirect

European Journal of Medicinal Chemistry

journal homepage: http://www.elsevier.com/locate/ejmech

Original article

Novel ^{18}F-labeled dibenzylideneacetone derivatives as potential positron emission tomography probes for *in vivo* imaging of β-amyloid plaques

Zijing Li [a], Mengchao Cui [a, *], Jinming Zhang [a, b, **], Jiapei Dai [c], Xiaojun Zhang [b], Peng Chen [a], Hongmei Jia [a], Boli Liu [a]

[a] Key Laboratory of Radiopharmaceuticals, Ministry of Education, College of Chemistry, Beijing Normal University, Beijing 100875, PR China
[b] Department of Nuclear Medicine, Chinese PLA General Hospital, Beijing 100853, PR China
[c] Wuhan Institute for Neuroscience and Neuroengineering, South-Central University for Nationalities, Wuhan 430074, PR China

ARTICLE INFO

Article history:
Received 22 April 2014
Received in revised form
17 July 2014
Accepted 19 July 2014
Available online 21 July 2014

Keywords:
Dibenzylideneacetone derivatives
Aβ plaques
PET imaging agents
AD

ABSTRACT

A series of dibenzylideneacetones were synthesized and evaluated as imaging probes for β-amyloid plaques. They displayed high binding affinity to $A\beta_{1-42}$ aggregates ($K_i = 6.4$ for **8**, $K_i = 3.0$ for **9**), and the high binding were confirmed by *in vitro* autoradiography with AD human and transgenic mouse brain sections. Two of them were selected for ^{18}F-labeling directly on the benzene ring. In biodistribution experiments, [^{18}F]**8** and [^{18}F]**9** displayed high initial uptakes (9.29 ± 0.41 and 5.38 ± 0.68% ID/g) and rapid washouts from the normal brain ($brain_{2\ min}/brain_{60\ min}$ ratios of 21.6 and 13.4). These preliminary results suggest that [^{18}F]**8** and [^{18}F]**9** may be used as potential PET imaging agents for the detection of Aβ plaques in the brain.

1. Introduction

Alzheimer's disease (AD) is devastating the elderly population with dementia, loss of memory, cognitive impairment, and inability to carry out routine activities [1]. It is not only a profound health and emotional influence on affected individuals and their families, but also a substantial economic burden on society. Extraordinary efforts will be spend on both the prevention and the treatment of dementia in the following decades, since this illness is going to affect about 63 million people by 2030, and 114 million by 2050 worldwide [2]. Early treatment depends on early disease diagnosis. However, the clinical diagnosis of AD is based mainly on the examination of mental and cognitive status nowadays [3], and the confirmation of the disease is achieved only by the postmortem examination of brain tissues [4,5]. It has been well established that the major neuropathological characteristics of AD is the presence of senile plaques (SPs) and neurofibrillary tangles (NFTs). Furthermore, the extra cellular deposition of β-amyloid (Aβ) as SPs leading to the neuronal pathogenesis is currently considered the major pathological hallmark of AD brains [6,7]. Therefore, recent research efforts have been focused on noninvasive early visualization of Aβ plaques in living brain tissues to identify and further monitor individuals at risk for AD, as well as to assist in the evaluation of new anti-amyloid therapies currently under development [8–10].

Although several imaging techniques such as magnetic resonance imaging (MRI) [11–13], single photon emission computed tomography (SPECT) [14], and optical imaging [15–18] have been explored for the visualization of Aβ plaques in the past decade, Aβ plaque-specific positron emission tomography (PET) imaging remains the most successful noninvasive technique to date, which generated great anticipation and high hopes [10,19,20]. Vast array of PET ligands based on three categories of chemical groups have been reported, the thioflavin-T derivatives, the stilbene derivatives, and the aminonaphthyl derivatives [10,19] (Fig. 1). The first PET tracer specific for Aβ plaques was [^{11}C]-2-(4-(N-methylamino)phenyl)-6-hydroxybenzothiazol ([^{11}C]PIB) [21,22] through modification of thioflavin-T, but it has certain limitation that requires an on-site cyclotron because of short half-life of ^{11}C. An analogue of PIB, which demonstrates potential utility, [^{18}F]-2-(3-fluoro-4-(N-

* Corresponding author. Key Laboratory of Radiopharmaceuticals, Ministry of Education, College of Chemistry, Beijing Normal University, Beijing 100875, PR China.
** Corresponding author. Department of Nuclear Medicine, Chinese PLA General Hospital, Beijing 100853, PR China.
E-mail addresses: cmc@bnu.edu.cn (M. Cui), zhangjm301@163.com (J. Zhang).

http://dx.doi.org/10.1016/j.ejmech.2014.07.070
0223-5234/

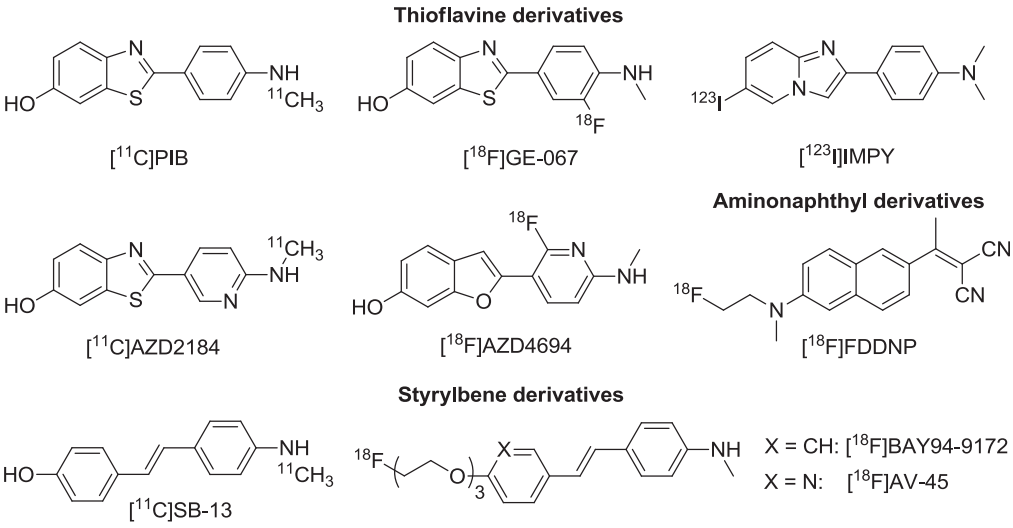

Fig. 1. Chemical structures of reported ^{18}F labeled Aβ imaging probes.

methylamino)phenyl)benzo[d]thiazol-6-ol ([^{18}F]GE-067) [23] has been tested clinically and approved by FDA. The stilbene derivatives include [^{11}C]-4-N-methylamino-4′-hydroxystilbene ([^{11}C]SB-13) [24,25], [^{18}F]-4-(N-methylamino)-4′-(2-(2-(2-fluoroethoxy) ethoxy)ethoxy)-stilbene ([^{18}F]BAY94-9172) [26] and [^{18}F]-(*E*)-4-(2-(6-(2-(2-(2-fluoroethoxy)ethoxy)ethoxy)pyridin-3-yl)vinyl)-N-methylaniline ([^{18}F]AV-45) [27,28], which are currently under commercial development for the mapping of Aβ plaque burden in living brain tissue. Among them, [^{18}F]AV-45 was the first Aβ tracer approved by FDA. The aminonaphthyl derivative [^{18}F]-2-(1-(2-(N-(2-fluoroethyl)-N-methylamino)-naphthalene-6-yl)ethylidene) malononitrile ([^{18}F]FDDNP) was the first PET ligand put into human trials and also reported to bind to NFTs [29–31], whose binding site on Aβ deposits may differ from those of the prior two categories [10]. However, almost all ^{18}F-labeled tracers currently in late phases of clinical development have high nonspecific white matter uptakes that give a distinctive white matter pattern in scans of healthy subjects. Furthermore, in PET scan images of AD patients, those ^{18}F-labeled tracers frequently show the gray matter–white matter demarcation loss, and consequent loss of the normal white matter pattern, which are the predominant evidence of cortical amyloid plaques [32]. In the cortical ribbon typical of a positive [^{11}C]PIB scan, it less often shows the clearly intense binding, too [32]. So, new probes beyond the above three categories with improved properties including higher affinity for Aβ plaques and less nonspecific binding in the white matter of the brain are always expected.

In 2010, an extensive set of dibenzylideneacetone derivatives was synthesized and screened for affinity toward Aβ_{1-42} aggregates by Cui et al. [33] Structure activity relationships revealed the binding of dibenzylideneacetones at the *para* position was highly tolerant of sterically demanding substitutions (K_i ranging from 0.9 to 7.0 nM). Two of them were labeled with ^{18}F through a short length of polyethylene glycol chain (PEG). In biodistribution experiments, the radiofluorinated ligands [^{18}F]**1** and [^{18}F]**2** exhibited good initial penetration (4.13 and 5.15% ID/g, respectively, at 2 min) of and ordinary clearance from the brain. The brain$_{2\ min}$/brain$_{60\ min}$ ratio of them is acceptable (4.59, and 4.06 for [^{18}F]**1**, and [^{18}F]**2**, respectively). These preliminary results suggested that the dibenzylideneacetone structure to be a potential new scaffold for the development of Aβ imaging probes.

Therefore, based on the backbone of dibenzylideneacetones and their known affinities for Aβ aggregates, in the present study we designed a new type of ^{18}F-labeled dibenzylideneacetone derivative (Fig. 2) for Aβ imaging using a novel ^{18}F-labeling approach in two steps. This pathway labels ^{18}F atom directly on the benzene ring in order to keep the affinity of dibenzylideneacetone to the greatest extent. Meanwhile, we also expect this innovation could minimize the molecular weight and improve the properties of the tracers, such as high brain uptakes, ineligible defluorination and better brain pharmacokinetics, compared with using the PEG pathway.

2. Results and discussion

2.1. Chemistry

The dibenzylideneacetone derivatives used in the binding assays and characterization of the corresponding ^{18}F-labeled ligands were produced following the synthetic route shown in Scheme 1. The two substituted (*E*)-4-phenylbut-3-en-2-one derivatives **4** and **5** were prepared according to the method described previously [33]. The dibenzylideneacetone derivatives were obtained through base-catalyzed Claisen condensation reactions that coupled the suitably substituted (*E*)-4-phenylbut-3-en-2-one with 4-flourobenzaldehyde or 2-flourpyridine-5-carboxaldehyde. The unsymmetrically substituted dibenzylideneacetones **7**, **8** and **9** were obtained in 85.0–90.5% yields, and their corresponding pyridine substituted compounds **10**, **11** and **12** were obtained in 78.3–88.9% yields. It should be mentioned here that we first used ethanol as the solvent for Claisen condensation reaction when preparing the pyridine derivatives **10**–**12**, but it turned out that the fluorine atom of the aimed product was displaced by ethoxy group (compounds **13**–**15**) at ambient temperature using K_2CO_3 as base and ethanol as solvent. The aromatic halides usually undergo nucleophilic substitution by various nucleophiles, such as secondary amines and alcoholate ion (e.g. ethanol as nucleophilic reagent at base condition), and the reaction rate will be accelerate when the fluoro atom was substituted at the *ortho* position of the pyridine ring. Therefore, we tried several different aprotic solvents such as acetonitrile, 1,4-dioxane, diethyl ether, DMF and THF to proceed this reaction, and we found DMF is an efficient solvent in this kind of condensation reaction, compound **10**–**12** were obtained with high yields (78.3–88.9%). It means that we should be very careful to choose the solvent when labeling the pyridine array compounds.

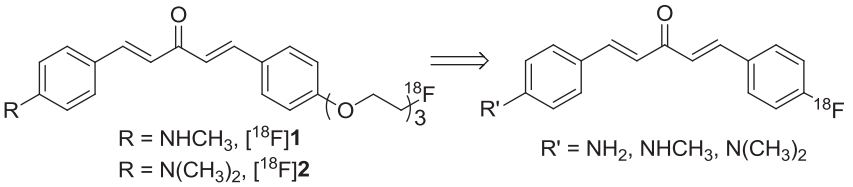

Fig. 2. Chemical structures of the designed ^{18}F labeled ligands in this work.

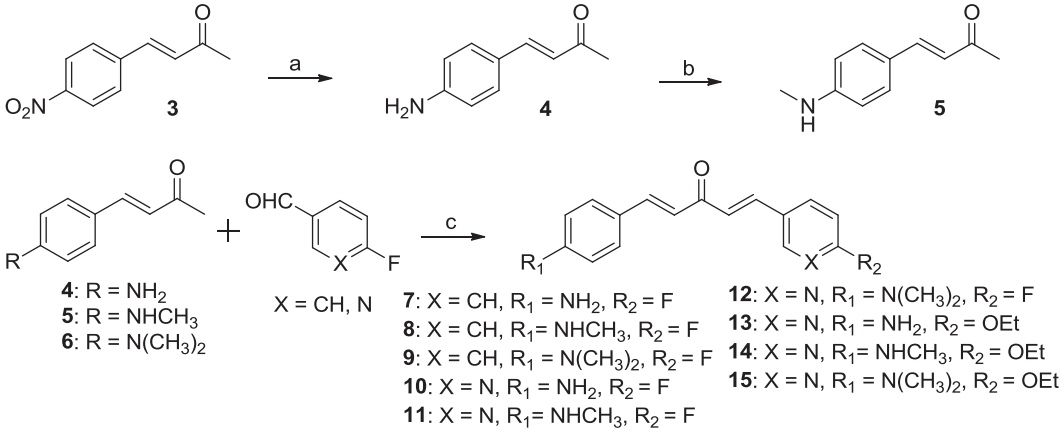

Scheme 1. Reagents and conditions: a. $SnCl_2 \cdot 2H_2O$, EtOH, HCl, reflux; b. K_2CO_3, CH_3I, r.t.; c. NaOH, EtOH, r.t. for **7**–**9** and **13**–**15**; NaOH, DMF, r.t. for **10**–**12**.

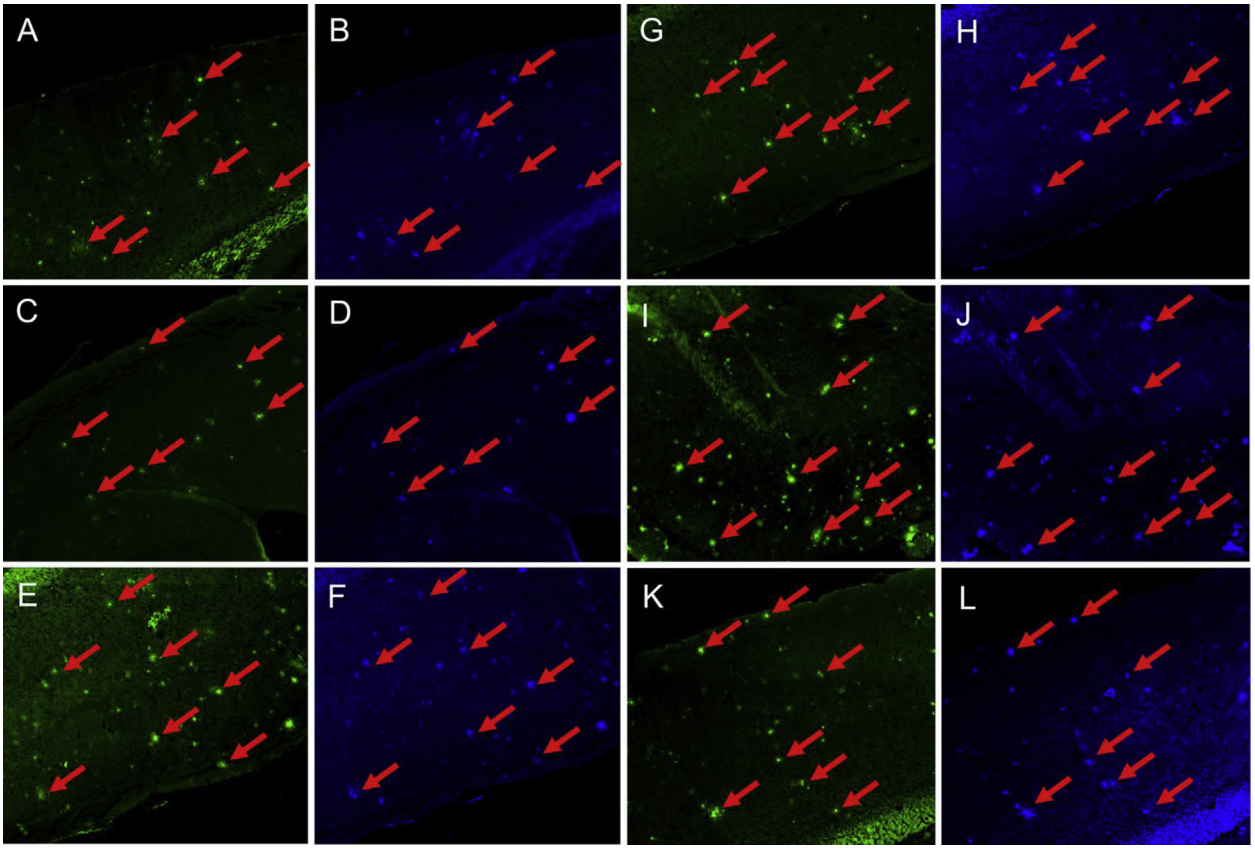

Fig. 3. *In vitro* fluorescent staining of compound **7**–**12** (A, C, E, G, I, K, respectively, with filter set of GFP) on brain sections of a Tg model mouse (C57BL6, APPswe/PSEN1, 11 months old, male), and thioflavin-S on the adjacent sections (B, D, F, H, J, L, respectively, with filter set of DAPI). Stained plaques are indicated by red arrows. (For interpretation of the references to color in this figure legend, the reader is referred to the web version of this article.)

2.2. In vitro fluorescent staining

To evaluate the binding affinities of compounds **7**–**12** to Aβ plaques, *in vitro* fluorescent staining of Aβ plaques on sections of brain tissue from Tg model mice (C57BL6, APPswe/PSEN1, 11 months old) were conducted as stated. As shown in Fig. 3 A, C, E, G, I and K, specific staining of plaques was clearly observed on the brain section of Tg mice for compound **7**–**12**. The presence and distribution of Aβ plaques were perfectly consistent with the results of staining applying thioflavin-S (a common dye for staining of Aβ plaques) on the adjacent sections (B, D, F, H, J and L).

2.3. In vitro binding studies

The quantitative affinities of these dibenzylideneacetone derivatives (**7**–**15**) for Aβ_{1-42} aggregates were examined in competition binding assays, using [^{125}I]-6-iodo-2-(4′-dimethylamino-) phenyl-imidazo[1,2]pyridine ([^{125}I]IMPY) as the competing radioligand. IMPY was also screened employing the same system for comparison. As illustrated in Table 1, all compounds inhibited the binding of [^{125}I]IMPY in a dose-dependent manner (Fig. 4) and displayed high binding affinities to Aβ_{1-42} aggregates with K_i values varied from 3.0 to 135.2 nM. Consistently to the previously reported findings, the tertiary *N*,*N*-dimethylamino analogues have higher affinities than the corresponding secondary *N*-methylamino analogues [34] (e.g., **8** vs. **9**, **11** vs. **12**). On the basis of the higher binding affinities to Aβ_{1-42} aggregates, compounds **8** ($K_i = 6.4 \pm 3.2$ nM) and **9** ($K_i = 3.0 \pm 0.6$ nM) were selected for ^{18}F labeling.

2.4. Radiolabeling

As shown in Scheme 2, in the first step of this two-step reaction, the ^{18}F-labled intermediate [^{18}F]-4-fluorobenzaldehyde ([^{18}F]**17**) was prepared with an average radiochemical yield of 40–60% (no decay corrected) after Sep-Pak C18 cartridge (Waters) separation. Then [^{18}F]**17** was eluted out with ethanol to go through a base-catalyzed Claisen condensation in the ethanol with two corresponding substituted (*E*)-4-phenylbut-3-en-2-one separately to yield [^{18}F]**8** and [^{18}F]**9**. The radiochemical yields of [^{18}F]**8** and [^{18}F]**9** in the second step were about 50% (no decay corrected), resulting an average of 25% total yield with radiochemical purity greater than 95% after high performance liquid chromatography (HPLC) purification. The specific activities were estimated at approximately 160 GBq/μmol (at the end of synthesis), high enough for the following *in vitro* and *in vivo* studies. The chemical identities of the ^{18}F-labeled tracers were verified by comparison of the retention times with those of the nonradioactive standard compounds (Fig. 5).

Table 1
Inhibition constants (K_i, nM) for binding to aggregates of Aβ_{1-42} versus [^{125}I]IMPY.[a]

Compound	K_i (nM)
7	17.1 ± 4.3
8	6.4 ± 3.2
9	3.0 ± 0.6
10	135.2 ± 58.1
11	36.5 ± 23.9
12	8.5 ± 2.0
13	65.8 ± 17.8
14	14.2 ± 5.2
15	7.6 ± 3.9
IMPY	11.5 ± 2.5

[a] Measured in triplicate with results given as the mean ± SD.

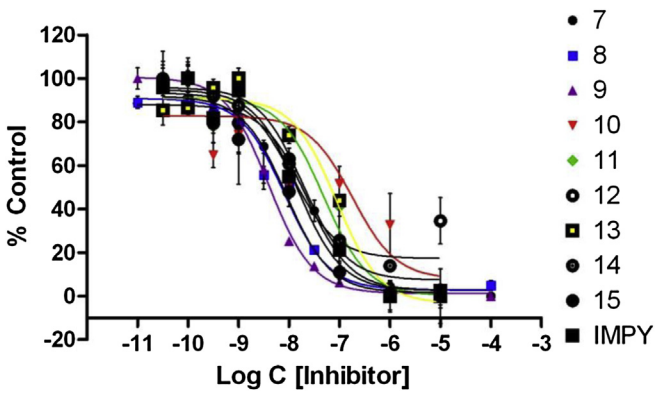

Fig. 4. Inhibition curves for the binding of [^{125}I]IMPY to Aβ_{1-42} aggregates.

We have two sound reasons to favor this two-step ^{18}F labeling strategy. First, the Claisen condensation for coupling was proved to be fast enough for ^{18}F labeling and a pretty convenient way to label ^{18}F on a benzene ring, a very important component in the core structure of dibenzylideneacetone. Second, this strategy is ready to be applied when labeling many other different molecules containing one ketone group in the future studies.

2.5. In vitro stability studies

[^{18}F]**8** and [^{18}F]**9** were found not only stable (>90%) in saline solution after storage for at least 1 h at room temperature during *in vitro* stability study, but also having high *in vitro* stability in mice plasma. After incubating for 60 min with mice plasma at 37 °C, more than 90% of the activity was identified as intact compound [^{18}F]**8** or [^{18}F]**9**, respectively.

2.6. In vitro autoradiography studies

Brain sections of a Tg mouse (C57BL6, APPswe/PSEN1, 11 months old) with Aβ plaques confirmed as well as an age-matched control mouse (C57BL6, 11 months old) were selected as staining material in the *in vitro* autoradiographic studies. As shown in Figs. 6 and 7, Aβ plaques of both hippocampus and cortical regions of the Tg mouse were selectively labeled by the ^{18}F-labeled tracers [^{18}F]**8** and [^{18}F]**9**, separately, while no notable Aβ plaques was noticed on the brain of the control mouse. The consistent results of fluorescent staining stained by thioflavin-S further confirmed the distribution and pattern of those Aβ plaques. Since a previous report suggested that the configuration/folding of Aβ plaques in Tg mice might be different from the tertiary/quaternary structure of Aβ plaques in AD brains [35], we consider the binding information of new tracers for Aβ plaques in human AD brain even more important. As illustrated in Fig. 8, tracer [^{18}F]**9** with a dimethylamino group was tested for autoradiographic studies in sections of human brain tissue, and as we supposed, typical labeling pattern of Aβ plaques was also observed on the AD brain section. For no apparent labeling was observed in normal adult brain section in contrast, this result further proved its affinity to Aβ plaques from AD brain.

2.7. In vivo biodistribution studies

The log *D* values (2.69 ± 0.19 for [^{18}F]**8** and 3.89 ± 0.21 for [^{18}F]**9**, respectively) indicate that tracer [^{18}F]**8** and [^{18}F]**9** have moderate lipophilicity which is suitable for brain imaging. Here, we summarized the time-activity data on the brain permeation as well as the other organ distribution of the ^{18}F-labeled tracers acquired in

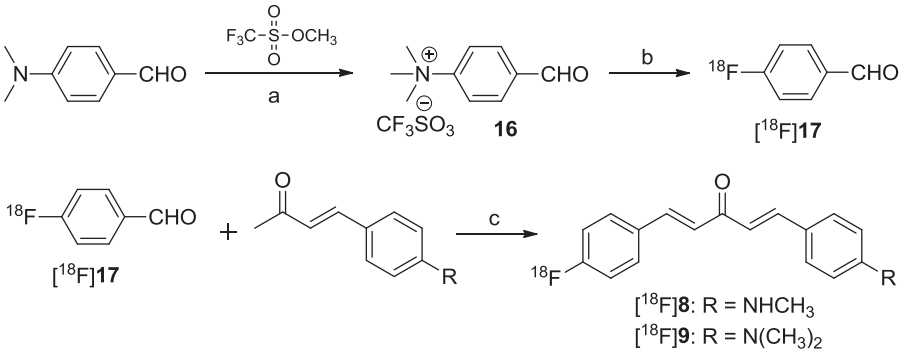

Scheme 2. Reagents and conditions: a. CH_2Cl_2, ice-salt bath; b. $K^{18}F$, K_{222}, DMSO, 160 °C, 6 min; c. NaOH, EtOH, r.t.

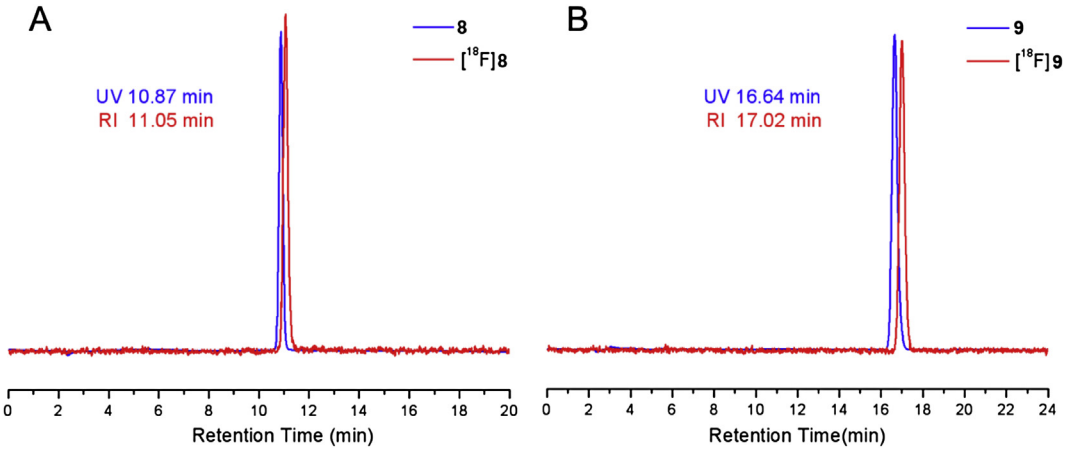

Fig. 5. (A) HPLC profiles of **8** and [^{18}F]**8**. (B) HPLC profiles of **9** and [^{18}F]**9**. HPLC conditions: Venusil MP C18 column (Agela Technologies, 10 × 250 mm), CH_3CN/H_2O = 70/30, 4 mL/min, UV = 254 nm.

biodistribution study in normal ICR mice in Tables 2 and 3. In this often used test to measure the initial brain uptake and washout kinetics from the normal brain, [^{18}F]**8** and [^{18}F]**9** displayed high uptakes into the brain (9.29 ± 0.41 and 5.38 ± 0.68% ID/g, respectively) at 2 min post-injection and fast washout kinetics from the healthy brain (0.43 ± 0.14 and 0.40 ± 0.07% ID/g at 60 min, respectively), which are comparable to those reported for the ^{18}F-labeled dibenzylideneacetone derivatives with PEG chains [33]. The ratio of $brain_{2\ min}/brain_{60\ min}$ is also considered as an important index to select tracers with appropriate kinetics *in vivo*. Based on this point, the washout of [^{18}F]AV-45 in healthy mice, with a $brain_{2\ min}/brain_{60\ min}$ ratios of 3.90 (7.33 ± 1.54% ID/g at 2 min, 1.88 ± 0.14% ID/g at 60 min) [27], is still not ideal, so as the recently reported ^{18}F labeled 2-pyridinyl benzoxazole and benzothiazole derivatives [36], with $brain_{2\ min}/brain_{60\ min}$ ratios ranged from 1.77 to 4.95. However, these two tracers showed $brain_{2\ min}/brain_{60\ min}$ ratios of 21.6 and 13.4, respectively, indicating that these new type of ^{18}F-labeled dibenzylideneacetone derivatives without the PEG chain may lower nonspecific white matter uptake. We also observed that *in vivo* defluorination which is an annoying problem with many ^{18}F-labeled tracers was very slightly occurring with [^{18}F]**8** and [^{18}F]**9**, because the increase of the bone uptakes with time were minimal, thus the interference of defluorination with the imaging is expected to be relatively minor. Additionally, these ^{18}F-labeled tracers also distributed to several other organs like the liver and the kidneys, However, their high initial uptakes were followed by moderate washouts. In summary, these two ^{18}F-labeled derivatives ([^{18}F]**8** and [^{18}F]**9**) meet the preliminary requirements for *in vivo* detection of Aβ plaques as potential PET imaging agents. Compared with the ^{18}F-labeled dibenzylideneacetone derivatives with PEG chains, the ^{18}F-labeled dibenzylideneacetone derivatives without PEG chains had greatly improved pharmacokinetics and may lower nonspecific white matter uptake.

3. Conclusions

In conclusion, a series of dibenzylideneacetone derivatives was prepared using straightforward chemistry and evaluated as new PET imaging tracers for Aβ plaques successfully. These dibenzylideneacetone derivatives tracers displayed various binding affinities to Aβ aggregates varied from 3.0 to 135.2 nM in the binding studies. Among them, two ligands with high affinities (K_i = 6.4 ± 3.2 nM for **8** and K_i = 3.0 ± 0.6 nM for **9**) to the aggregated Aβ were selected for ^{18}F labeling and further evaluation. At first, the high affinities of these two tracers were again confirmed in the *in vitro* autoradiography on sections of postmortem AD brain and Tg mouse brain. Then, in biodistribution experiments, both radiotracers [^{18}F]**8** and [^{18}F]**9** displayed high initial uptakes into (9.29 ± 0.41 and 5.38 ± 0.68% ID/g at 2 min, respectively) and very rapid washouts from the brain in normal mice ($brain_{2\ min}/brain_{60\ min}$ ratios of 21.6 and 13.4, respectively), indicating the pharmacokinetics had been greatly improved by these ^{18}F-labeled dibenzylideneacetone derivatives without PEG chains. All the above results tell those two components, **8** and **9**, are highly desirable for Aβ imaging because they may have much lower nonspecific white matter uptake. Furthermore, more than 90% of the activity was identified as the

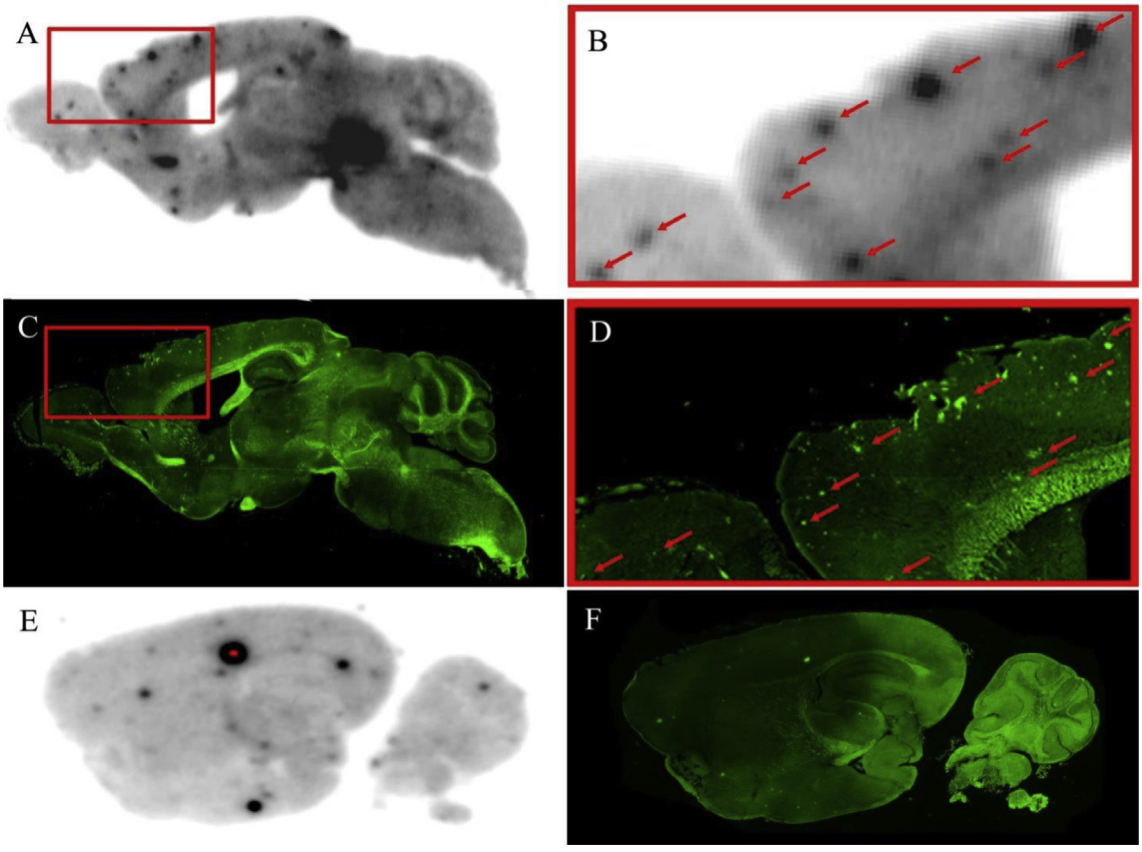

Fig. 6. (A, B) *In vitro* autoradiography of [^{18}F]**8** on a Tg model mouse (C57BL6, APPswe/PSEN1, 11 months old, male). (C, D) The presence and distribution of plaques were confirmed by fluorescence staining using thioflavin-S on the same section with a filter set for GFP. (E) *In vitro* autoradiography of [^{18}F]**8** on a brain section of a age matched normal mouse as control. (F) Fluorescence staining using thioflavin-S on the same section of control mouse.

intact tracer respectively after 60 min incubating with either saline solution or mice plasma at 37 °C, indicating that both [^{18}F]**8** and [^{18}F]**9** displayed high *in vitro* stability. Overall, [^{18}F]**8** and [^{18}F]**9** with ^{18}F directly labeled on the benzene ring of dibenzylideneacetone derivatives are promising PET agents for imaging cerebral Aβ plaques, and further evaluation in model animal and human subjects with PET would provide valuable data for further Aβ tracer designation and development.

4. Experimental

4.1. General information

All the reagents we used in the synthesis were commercially available and were used without further purification unless otherwise indicated. The ^{1}H NMR spectra and ^{13}C NMR were obtained at a 400 MHz on Bruker spectrometer with samples dissolved in $CDCl_3$ solutions at room temperature. TMS was used as an internal standard, and all the chemical shifts were reported as δ values relative to the internal TMS. The coupling constants were reported in Hertz. Multiplicity is defined by s (singlet), d (doublet), t (triplet), and m (multiplet). Mass spectrometry was acquired under the Surveyor MSQ Plus (ESI) (Waltham, MA, USA) instrument. The synthesis reactions were carefully monitored by TLC (TLC Silica gel 60 F_{254} aluminum sheets, Merck), because compounds were all visualized when illuminated with a short wavelength UV lamp (λ = 254 nm). Column chromatography purifications were performed on silica gel (54–74 μm, Qingdao Haiyang Chemical Co., Ltd.). Radiochemical purity was evaluated by HPLC analysis performed on a Shimadzu system SCL-20 AVP equipped with a SPD-20A UV detector (λ = 254 nm) as well as a Bioscan Flow Count 3200 NaI/PMT γ-radiation scintillation detector. HPLC separations were achieved on a Venusil MP C18 reverse phase column (Agela Technologies, 5 μm, 10 mm × 250 mm) eluted with a binary gradient system at a flow rate of 4.0 mL/min on the Shimadzu HPLC; and HPLC analysis were achieved on a Venusil MP C18 reverse phase column (Agela Technologies, 5 μm, 4.6 mm × 250 mm) eluted with a binary gradient system at a flow rate of 1.0 mL/min also with the Shimadzu HPLC. Mobile phase A was deionized water while mobile phase B was HPLC grade acetonitrile purchased from Amethyst Chemicals. The purities of the synthesized standard compounds (**8** and **9**) was determined using analytical HPLC and was found to be higher than 98%. Fluorescent observation was performed on the Observer Z1 (Zeiss, Germany) equipped with a DAPI filter set (excitation, 375 nm) and a GFP filter set (excitation, 488 nm). The normal ICR mice (five weeks, male) we used for biodistribution experiments were purchased from the Department of Laboratory Animal Science, Peking University Health Science Center. The Alzheimer's animal model, a transgenic mouse (C57BL6, APPswe/PSEN1, 11 months old) and an age-matched control mouse (C57BL6, 11 months old) were purchased from the Institute of Laboratory Animal Science, Chinese Academy of Medical Sciences. All protocols in this project requiring the use of mice were under approval by the animal care committee

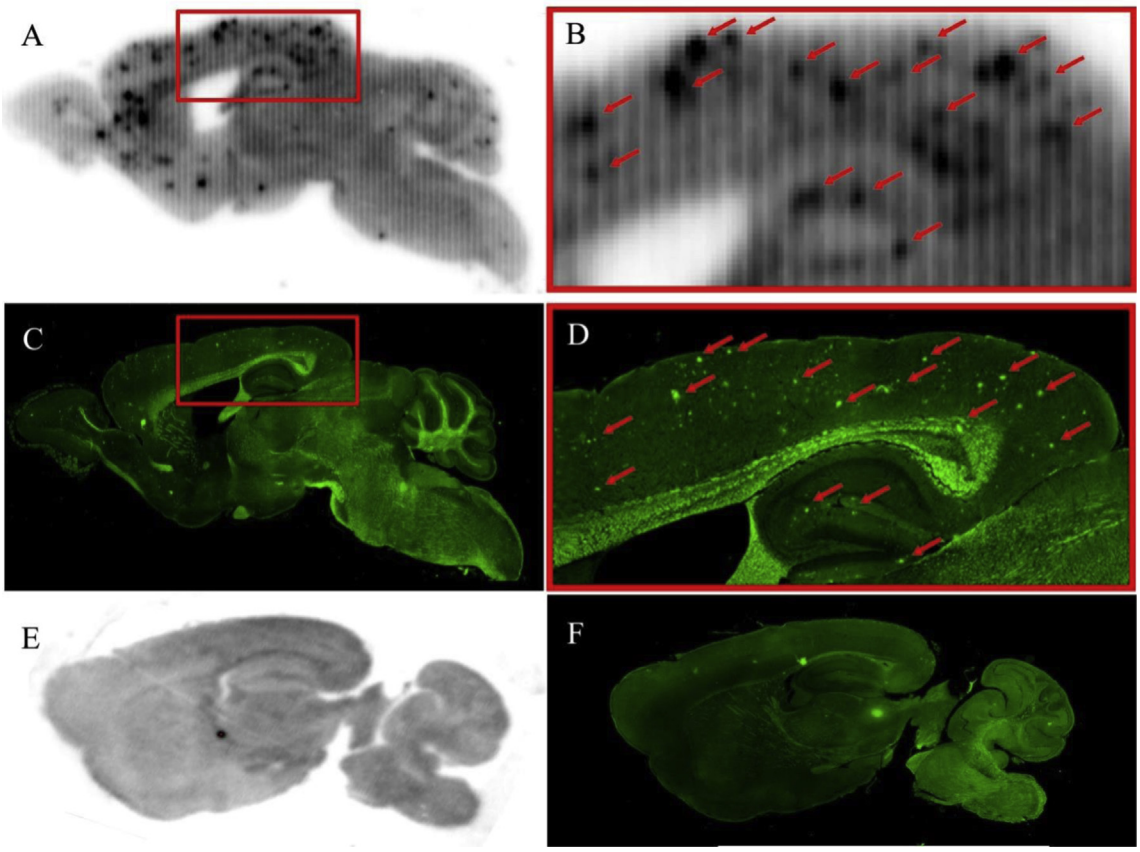

Fig. 7. (A, B) *In vitro* autoradiography of [^{18}F]**9** on a Tg model mouse (C57BL6, APPswe/PSEN1, 11 months old, male). (C, D) The presence and distribution of plaques were confirmed by fluorescence staining using thioflavin-S on the same section with a filter set for GFP. (E) *In vitro* autoradiography of [^{18}F]**9** on a brain section of a age matched normal mouse as control. (F) Fluorescence staining using thioflavin-S on the same section of control mouse.

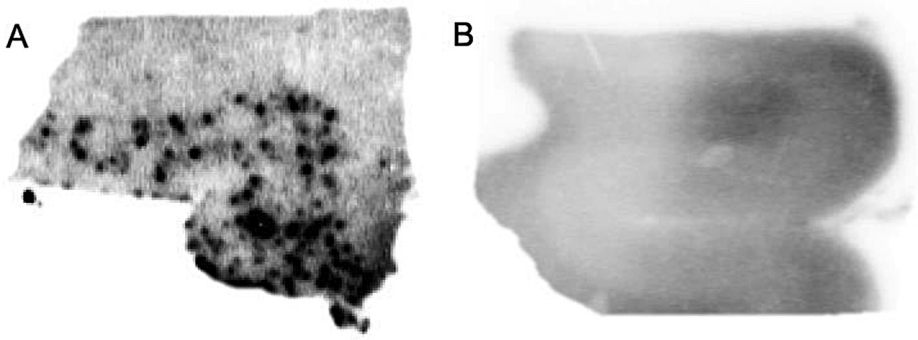

Fig. 8. (A) *In vitro* autoradiography of [^{18}F]**9** on an AD patient (64 years old, female) and (B) a normal person (74 years old, male) as control.

of Beijing Normal University. Post-mortem brain tissues from an AD case (64 years old, female) and a control case (74 years old, male) were obtained from the Chinese Brain Bank Center.

*4.2. (1E, 4E)-1-(4-Aminophenyl)-5-(4-fluorophenyl)penta-1,4-dien-3-one (**7**)*

Dissolve compound **4** (161 mg, 1 mmol) and 4-fluorobenzaldehyde (124 mg, 1 mmol) in 5 mL ethanol and add NaOH (40 mg, 1 mmol). The solution was stirred for 10 min at room temperature, and yellow solids precipitated from the solution. Keep the reaction for another 1 h. Final product was collected by filtration and washing by petroleum ether. The residue was purified by chromatography (ethylacetate/petroleum ether = 1:1, v/v) to afford yellow solid (yield 85.0%). ^{1}H NMR ($CDCl_3$, 400 MHz): δ 4.07 (s, 2H), 7.68 (d, J = 8.0 Hz, 2H), 6.87 (d, J = 15.6 Hz, 1H), 7.00 (d, J = 16.0 Hz, 1H), 7.09 (t, J = 8.4 Hz, 2H), 7.45 (d, J = 8.4 Hz, 2H), 7.59 (dd, J_1 = 8.7 Hz, J_2 = 2.3 Hz, 2H), 7.67 (d, J = 16.0 Hz, 1H), 7.68 (d, J = 15.6 Hz, 1H). ^{13}C NMR ($CDCl_3$, 100 MHz): δ 114.9, 115.9, 116.2, 121.6, 124.9, 125.5, 130.1, 130.5, 141.0, 144.1, 149.2, 162.6, 165.1, 188.7. HRMS (TOF MS ES$^+$): m/z calcd for $C_{17}H_{15}NOF^+$ 268.1132 $[M+H]^+$; found 268.1139.

*4.3. (1E, 4E)-1-(4-Fluorophenyl)-5-(4-(methylamino)phenyl) penta-1,4-dien-3-one (**8**)*

Compound **8** was prepared following the procedure used for **7**. The residue was purified by chromatography (ethylacetate/

Table 2
Biodistribution of [^{18}F]**8** in male ICR mice.[a]

Organ	Time after injection			
	2 min	10 min	30 min	60 min
Blood	5.08 ± 1.49	3.75 ± 0.81	3.71 ± 1.24	2.53 ± 0.84
Brain	9.29 ± 0.41	1.65 ± 0.23	0.56 ± 0.06	0.43 ± 0.14
Heart	8.57 ± 0.67	2.97 ± 0.34	1.77 ± 0.28	1.27 ± 0.31
Liver	15.72 ± 1.21	21.29 ± 1.90	15.26 ± 1.94	10.74 ± 0.80
Spleen	4.29 ± 0.72	2.20 ± 0.28	1.64 ± 0.30	1.27 ± 0.38
Lung	23.90 ± 3.21	12.90 ± 1.63	8.99 ± 1.93	6.32 ± 0.99
Kidney	17.19 ± 1.11	18.19 ± 4.68	16.07 ± 4.42	12.57 ± 0.58
Pancreas	9.95 ± 0.39	3.49 ± 0.54	2.12 ± 0.28	1.43 ± 0.39
Bone	1.87 ± 0.33	0.42 ± 0.08	1.30 ± 0.70	2.20 ± 0.72
Stomach[b]	2.93 ± 0.48	5.17 ± 0.55	5.22 ± 1.19	2.28 ± 0.63
Small intestine[b]	9.74 ± 1.01	10.25 ± 5.62	31.22 ± 5.02	55.10 ± 10.58

[a] Expressed as % injected dose per gram. Average for 5 mice ± standard deviation.
[b] Expressed as % injected dose per organ.

Table 3
Biodistribution of [^{18}F]**9** in male ICR mice.[a]

Organ	Time after injection			
	2 min	10 min	30 min	60 min
Blood	6.89 ± 1.52	4.44 ± 0.77	5.56 ± 0.91	2.80 ± 0.42
Brain	5.38 ± 0.68	1.27 ± 0.14	0.55 ± 0.09	0.40 ± 0.07
Heart	9.86 ± 1.81	2.65 ± 0.23	1.98 ± 0.58	1.16 ± 0.18
Liver	16.32 ± 4.34	15.37 ± 0.58	6.94 ± 0.89	7.94 ± 0.11
Spleen	3.32 ± 0.43	1.47 ± 0.19	1.16 ± 0.32	0.61 ± 0.18
Lung	8.96 ± 1.74	4.82 ± 0.07	3.79 ± 1.00	2.51 ± 0.35
Kidney	17.02 ± 1.00	13.96 ± 2.38	15.98 ± 3.64	12.23 ± 4.31
Pancreas	7.16 ± 0.86	2.83 ± 0.48	2.40 ± 0.33	1.08 ± 0.16
Bone	2.42 ± 0.51	1.23 ± 0.49	0.92 ± 0.46	1.09 ± 0.27
Stomach[b]	2.04 ± 0.25	2.54 ± 0.46	3.11 ± 0.73	2.28 ± 0.13
Small intestine[b]	6.52 ± 2.77	7.41 ± 2.83	12.67 ± 1.76	31.18 ± 9.47

[a] Expressed as % injected dose per gram. Average for 5 mice ± standard deviation.
[b] Expressed as % injected dose per organ.

petroleum ether = 1:2, v/v) to afford yellow solid (yield 87.6%). ^{1}H NMR ($CDCl_3$, 400 MHz): δ 2.90 (s, 3H), 6.60 (d, J = 8.4 Hz, 2H), 6.85 (d, J = 15.6 Hz, 1H), 7.01 (d, J = 16.0 Hz, 1H), 7.09 (t, J = 8.6 Hz, 2H), 7.48 (d, J = 8.8 Hz, 2H), 7.60 (dd, J_1 = 8.8 Hz, J_2 = 5.6 Hz, 2H), 7.67 (d, J = 15.6 Hz, 1H), 7.70 (d, J = 15.60 Hz, 1H). ^{13}C NMR ($CDCl_3$, 100 MHz): δ 30.3, 112.2, 115.9, 116.1, 120.9, 123.5, 125.5, 130.1, 130.6, 140.7, 144.5, 151.5, 162.8, 164.8, 188.7. HRMS (TOF MS ES$^+$): m/z calcd for $C_{18}H_{17}NOF^+$ 282.1289 $[M+H]^+$; found 282.1291.

*4.4. (1E, 4E)-1-(4-(Dimethylamino)phenyl)-5-(4-fluorophenyl) penta-1,4-dien-3-one (**9**)*

Compound **9** was prepared following the procedure used for **7**. The residue was purified by chromatography (ethylacetate/petroleum ether = 1:3, v/v) to afford yellow solid (yield 90.5%). ^{1}H NMR ($CDCl_3$, 400 MHz): δ 3.06 (s, 3H), 6.72 (d, J = 8.9 Hz, 2H), 6.88 (d, J = 15.7 Hz, 1H), 7.04 (d, J = 15.9 Hz, 1H), 7.11 (t, J = 8.6 Hz, 2H), 7.54 (d, J = 8.9 Hz, 2H), 7.62 (dd, J_1 = 8.7 Hz, J_2 = 5.4 Hz, 2H), 7.69 (d, J = 15.9 Hz, 1H), 7.74 (d, J = 15.8 Hz, 1H). ^{13}C NMR ($CDCl_3$, 100 MHz): δ 40.1, 111.9, 115.9, 116.1, 120.9, 122.5, 125.6, 130.1, 130.5, 140.6, 144.4, 152.1, 162.6, 165.1, 188.6. HRMS (TOF MS ES$^+$): m/z calcd for $C_{19}H_{19}NOF^+$ 296.1445 $[M+H]^+$; found $C_{19}H_{19}NOF^+$ 296.1450.

*4.5. (1E, 4E)-1-(4-Aminophenyl)-5-(6-fluoropyridin-3-yl)penta-1,4-dien-3-one (**10**)*

Dissolve compound **4** (161 mg, 1 mmol) and 6-fluoropyridine-3-carbaldehyde (125 mg, 1 mmol) in 5 mL DMF and add NaOH (40 mg, 1 mmol). The solution was stirred for 1 h at room temperature, and yellow solids precipitated from the solution. Keep the reaction for another 1 h. Final product was collected by filtration and washing by petroleum ether. The residue was purified by silica gel chromatography (ethylacetate/petroleum ether = 1:1, v/v) to afford yellow solid (yield 78.3%). ^{1}H NMR ($CDCl_3$, 400 MHz): δ 4.07 (s, 2H), 6.68 (d, J = 8.4 Hz, 2H), 6.87 (d, J = 15.8 Hz, 1H), 7.00 (dd, J_1 = 8.5 Hz, J_2 = 2.7 Hz, 1H), 7.07 (d, J = 15.9 Hz, 1H), 7.46 (d, J = 8.4 Hz, 2H), 7.68 (t, J = 15.3 Hz, 2H), 8.01–8.06 (m, 1H), 8.43 (s, 1H). ^{13}C NMR ($CDCl_3$, 100 MHz): δ 111.7, 114.9, 121.6, 124.7, 130.5, 130.6, 136.5, 138.8, 144.0, 148.8, 149.2, 165.1, 188.5. HRMS (TOF MS ES$^+$): m/z calcd for $C_{16}H_{13}N_2OF^+$ 269.1085 $[M+H]^+$; found 269.1107.

*4.6. (1E, 4E)-1-(6-Fluoropyridin-3-yl)-5-(4-(methylamino)phenyl) penta-1,4-dien-3-one (**11**)*

Compound **11** was prepared following the procedure used for **10**. The residue was purified by chromatography (ethylacetate/petroleum ether = 1:2, v/v) to afford yellow solid (yield 83.2%). ^{1}H NMR ($CDCl_3$, 400 MHz): δ 2.90 (s, 3H), 4.24 (s, 1H), 6.60 (d, J = 8.4 Hz, 2H), 6.84 (d, J = 15.7 Hz, 1H), 6.99 (dd, J_1 = 8.5 Hz, J_2 = 2.6 Hz, 1H), 7.08 (d, J = 15.9 Hz, 1H), 7.48 (d, J = 8.4 Hz, 2H), 7.66 (d, J = 15.9 Hz, 1H), 7.72 (d, J = 15.8 Hz, 1H), 8.01–8.05 (m, 1H), 8.42 (s, 1H). ^{13}C NMR ($CDCl_3$, 100 MHz): δ 30.3, 109.9, 112.3, 123.3, 127.3, 130.3, 130.7, 136.6, 139.4, 145.2, 148.2, 151.7, 165.1, 188.1. HRMS (TOF MS ES$^+$): m/z calcd for $C_{17}H_{15}N_2OF^+$ 283.1241 $[M+H]^+$; found 283.1260.

*4.7. (1E, 4E)-1-(4-(Dimethylamino)phenyl)-5-(6-fluoropyridin-3-yl)penta-1,4-dien-3-one (**12**)*

Compound **12** was prepared following the procedure used for **10**. The residue was purified by silica gel chromatography (ethylacetate/petroleum ether = 1:3, v/v) to afford yellow solid (yield 88.9%). ^{1}H NMR ($CDCl_3$, 400 MHz): δ 3.07 (s, 6H), 6.73 (d, J = 7.9 Hz, 2H), 6.86 (d, J = 15.7 Hz, 1H), 7.01 (dd, J_1 = 8.5 Hz, J_2 = 2.8 Hz, 1H), 7.10 (d, J = 15.9 Hz, 1H), 7.54 (d, J = 8.8 Hz, 2H), 7.67 (d, J = 15.9 Hz, 1H), 7.75 (d, J = 15.7 Hz, 1H), 8.03–8.07 (m, 1H), 8.44 (s, 1H). ^{13}C NMR ($CDCl_3$, 100 MHz): δ 40.1, 111.6, 111.9, 120.8, 122.5, 124.4, 124.7, 130.4, 136.5, 138.4, 144.3, 148.7, 165.0, 188.4. HRMS (TOF MS ES$^+$): m/z calcd for $C_{18}H_{17}N_2OF^+$ 297.1398 $[M+H]^+$; found 297.1431.

*4.8. (1E, 4E)-1-(4-aminophenyl)-5-(6-ethoxypyridin-3-yl)penta-1,4-dien-3-one (**13**)*

Compound **13** was prepared following the procedure used for **7**. The residue was purified by silica gel chromatography (ethylacetate/petroleum ether = 1:1, v/v) to afford yellow solid (yield 73.6%). ^{1}H NMR ($CDCl_3$, 400 MHz): δ 1.41 (t, J = 7.1 Hz, 3H), 4.06 (s, 2H), 4.40 (dd, J_1 = 14.1 Hz, J_2 = 7.0 Hz, 2H), 6.67 (d, J = 8.4 Hz, 2H), 6.76 (d, J = 8.7 Hz, 1H), 6.87 (d, J = 15.8 Hz, 1H), 6.96 (d, J = 15.9 Hz, 1H), 7.44 (d, J = 8.5 Hz, 2H), 7.65 (d, J = 15.8 Hz, 1H), 7.67 (d, J = 15.8 Hz, 1H), 7.85 (dd, J_1 = 8.7 Hz, J_2 = 2.4 Hz, 1H), 8.32 (d, J = 2.2 Hz, 1H). ^{13}C NMR ($CDCl_3$, 100 MHz): δ 14.6, 62.3, 111.7, 114.9, 121.5, 124.7, 130.2, 130.4, 130.5, 136.5, 138.8, 144.1, 148.8, 149.2, 165.0, 188.5. HRMS (TOF MS ES$^+$): m/z calcd for $C_{18}H_{19}N_2O_2^+$ 295.1441 $[M+H]^+$; found 295.1436.

*4.9. (1E, 4E)-1-(6-ethoxypyridin-3-yl)-5-(4-(methylamino)phenyl) penta-1,4-dien-3-one (**14**)*

Compound **14** was prepared following the procedure used for **7**. The residue was purified by silica gel chromatography (ethylacetate/petroleum ether = 1:2, v/v) to afford yellow solid (yield 83.4%). ^{1}H NMR ($CDCl_3$, 400 MHz): δ 1.41 (t, J = 7.0 Hz, 3H), 2.89 (s, 3H), 4.40 (dd, J_1 = 14.1 Hz, J_2 = 7.0 Hz, 2H), 6.59 (d, J = 8.6 Hz, 2H),

6.76 (d, $J = 8.7$ Hz, 1H), 6.84 (d, $J = 15.8$ Hz, 1H), 6.97 (d, $J = 15.8$ Hz, 1H), 7.47 (d, $J = 8.6$ Hz, 2H), 7.69 (d, $J = 16.0$ Hz, 1H), 7.65 (d, $J = 16.0$ Hz, 1H), 7.84 (dd, $J_1 = 8.6$ Hz, $J_2 = 2.4$ Hz, 1H), 8.32 (d, $J = 2.1$ Hz, 1H). ^{13}C NMR ($CDCl_3$, 100 MHz): δ 14.6, 30.3, 62.3, 111.6, 112.2, 120.8, 123.6, 124.3, 124.7, 130.6, 136.5, 138.5, 144.4, 148.7, 151.5, 165.0, 188.5. HRMS (TOF MS ES$^+$): m/z calcd for $C_{19}H_{21}N_2O_2^+$ 309.1603 $[M+H]^+$; found 309.1542.

4.10. (1E, 4E)-1-(4-(dimethylamino)phenyl)-5-(6-ethoxypyridin-3-yl)penta-1,4-dien-3-one (**15**)

Compound **15** was prepared following the procedure used for **7**. The residue was purified by silica gel chromatography (ethylacetate/petroleum ether = 1:3, v/v) to afford yellow solid (yield 85.8%). ^{1}H NMR ($CDCl_3$, 400 MHz): δ 1.40 (t, $J = 7.1$ Hz, 3H), 3.02 (s, 6H), 4.40 (dd, $J_1 = 14.2$ Hz, $J_2 = 7.1$ Hz, 2H), 6.67 (d, $J = 8.8$ Hz, 2H), 6.75 (d, $J = 8.6$ Hz, 1H), 6.84 (d, $J = 15.7$ Hz, 1H), 6.97 (d, $J = 15.8$ Hz, 1H), 7.50 (d, $J = 8.8$ Hz, 2H), 7.64 (d, $J = 15.9$ Hz, 1H), 7.70 (d, $J = 15.7$ Hz, 1H), 7.84 (dd, $J_1 = 8.7$ Hz, $J_2 = 2.3$ Hz, 1H), 8.32 (d, $J = 2.2$ Hz, 1H). ^{13}C NMR ($CDCl_3$, 100 MHz): δ 14.6, 40.1, 62.2, 111.6, 111.9, 120.7, 122.4, 124.4, 124.7, 130.4, 136.4, 138.4, 144.3, 148.7, 152.0, 165.0, 188.4. MS (TOF MS ES$^+$): m/z calcd for $C_{20}H_{23}N_2O_2^+$ 323.1760 $[M+H]^+$; found 323.1804.

4.11. 4-(N, N, N-trimethylamino)benzaldehyde triflate (**16**)

Dissolve 4-dimethylaminobenzaldehyde (124 mg, 1 mmol) in 5 mL CH_2Cl_2 and add methyl trifluoromethanesulfonate (150 μL, 1.2 mmol) dropwise in ice salt bath. The solution was stirred for 3 h in the ice salt bath, and white solid precipitated from the solution. After filtration, washing with CH_2Cl_2, 75.7 mg white solid was obtained (yield 24.2%). ^{1}H NMR (D_2O, 400 MHz): δ 3.66 (s, 9H), 8.02 (d, $J = 9.0$ Hz, 2H), 8.13 (d, $J = 9.0$ Hz, 2H), 9.99 (s, 1H).

4.12. In vitro fluorescent staining of Aβ plaques on transgenic mouse brain sections

Before use, paraffin-embedded brain sections of Tg mouse (C57BL6, APPswe/PSEN1, 11 months old, male, 6 μm) were deparaffinized according to the following procedure: 2 × 20 min washes with xylene, 2 × 5 min washes with 100% ethanol, 5 min washes with 90% ethanol/H_2O, 5 min wash with 80% ethanol/H_2O, 5 min wash with 60% ethanol/H_2O, running tap water for 10 min, and then incubated in PBS buffer (0.2 M, pH = 7.4) for 30 min. The brain sections were then incubated with 10% (v/v) ethanol solution of **7**–**12** (1 μM) for 10 min at room temperature just before examining by microscope. The localization and patterns of Aβ plaques was confirmed by staining with thioflavin-S on the adjacent sections as contrast. For the staining of thioflavin-S, the deparaffinized sections were immersed in a thioflavin-S solution (0.125%, w/w) containing 10% EtOH (v/v) for 3 min and then washed with 40% EtOH. Finally, before examining by the microscope, the sections were washed again with 40% ethanol and PBS (0.2 M, pH = 7.4) for 10 min. Fluorescent observation was performed by microscope Observer Z1 (Zeiss, Germany) equipped with DAPI (excitation, 375 nm) and GFP filter sets (excitation, 488 nm).

4.13. In vitro binding assay to Aβ aggregates

The trifluoroacetic acid salt forms of peptides $A\beta_{1-42}$ were purchased from Osaka Peptide Institute (Osaka, Japan). Aggregation reaction was carried out by first gently dissolving the peptide (0.56 mg/mL for $A\beta_{1-42}$) in a buffer solution (pH = 7.4) which contained 10 mM sodium phosphate and 1 mM EDTA. The solution was incubated with gentle and constant shaking at 37 °C for 42 h. Inhibition experiments were carried out according to procedures described previously [37] with some modification. To be brief, 100 μL of aggregated Aβ fibrils (28 nM in the final assay mixture) was added to a mixture which contains 100 μL of radioligand ([^{125}I]IMPY, 100,000 cpm/100 μL), 100 μL of inhibitors (10^{-4}–$10^{-8.5}$ M in ethanol), and 700 μL of PBS (0.2 M, pH = 7.4) in a final volume of 1 mL in 12 mm × 75 mm borosilicate glass tubes. The mixture was incubated at room temperature for 3 h, and then, the bound and free radioactive fractions were separated by vacuum filtration through borosilicate glass fiber filters (Whatman GF/B) performed by a Mp-48T cell harvester (Brandel, Gaithersburg, MD). The radioactivity caught by the filters containing the bound ^{125}I-ligand was measured by a γ-counter (WALLAC/Wizard1470, United States) with about 70% efficiency. Under the assay conditions, the specifically bound fraction accounted for about 10% of total radioactivity. Nonspecific binding was defined in the presence of IMPY (1 μM) in the same way. The inhibitory concentration (IC_{50}) was determined using Graph Pad Prism 4.0 software. The inhibition constant (K_i) was calculated according to the Cheng-Prusoff inhibition constant equation: $K_i = IC_{50}/(1+[L]/K_d)$.

4.14. Radiolabeling

[^{18}F]Fluoride trapped on a QMA Light cartridge (Waters) was eluted with 1 mL of Kryptofix$_{222}$/K_2CO_3 solution (13 mg of Kryptofix$_{222}$ and 1.1 mg of K_2CO_3 in CH_3CN/H_2O, 4: 1 (v/v) into a clean glass vial. The solvent was quickly removed by heating at 120 °C under a stream of nitrogen gas. Then, the residue was azeotropically dried with 1 mL of anhydrous acetonitrile by three times (about 0.3 mL for each) at 120 °C under a stream of nitrogen gas. 4-(N, N, N-trimethylamino)benzaldehyde triflate (5.0 mg) dissolved in 1.0 mL of dry DMSO was added to the reaction vessel containing the $^{18}F^-$ activity and heated at 160 °C for 6 min. After the reaction vial was cooled by running cold water to room temperature, 10.0 mL of water were added to this orange solution. We passed the mixture with a syringe through a Sep-Pak C18 cartridge (Agela Technologies). The cartridge was washed with 10 mL of water, and the intermediate [^{18}F]-4-fluorobenzaldehyde was eluted with 1 mL of EtOH the [^{18}F]-4-fluorobenzaldehyde was washed out by 1 mL EtOH. The appropriate ketones (**5** or **6**, 1.0 mg) were added into the EtOH solution containing [^{18}F]-4-fluorobenzaldehyde, as well as 4.0 mg of NaOH to catalyze the Claisen condensation, the mixture was kept for 30 min with gentle shaking under room temperature. The longer the reaction was, the higher the condensation yields are found. But taking the decay into consideration, 30 min is better. The solvent was evaporated under nitrogen gas and the residue was dissolved in HPLC eluent and neutralized with 6 μL acetic acid before subjecting to HPLC for purification (Agela Technologies, 5 μm, 10 mm × 250 mm, CH_3CN/H_2O = 70/30; flow rate = 4 mL/min). After purification by HPLC, the radiochemical purity of [^{18}F]**8** and [^{18}F]**9** was greater than 95%. The retention time of [^{18}F]**8** and [^{18}F]**9** were 11.05 and 17.02 min in this HPLC system, respectively. The preparation took 90 min and the total radiochemical yield was about 25% (at the end of synthesis, no decay corrected).

4.15. In vitro autoradiography on brain sections of human and transgenic model mouse

The paraffin-embedded sections of human and transgenic model mouse brain were deparaffinized first with 2 × 20 min washes in xylene; then 2 × 5 min washes in 100% ethanol; 5 min wash in 90% ethanol/H_2O; 5 min wash in 80% ethanol/H_2O; 5 min wash in 60% ethanol/H_2O and finally 10 min wash in running tap water before incubating in PBS (0.2 M, pH = 7.4) for 30 min. The sections were then incubated with [^{18}F]**8** and [^{18}F]**9** (1.85 MBq/

200 μL) solution in saline for 1 h at room temperature. After they were rinsed with water for 1 min, washed with 40% EtOH, and dried with blowing air, the sections were exposed to a phosphorus plate (Perkin Elmer, USA) for 2 h in dark. *In vivo* autoradiographic images were obtained by a phosphor imaging system (Cyclone, Packard). After the *in vitro* autoradiographic examination, the same mouse brain sections were stained again by thioflavin-S solution the same way in *in vitro* fluorescent staining to confirm the presence and pattern of Aβ plaques. The fluorescent observation was performed on the Observer Z1 (Zeiss, Germany) equipped with GFP filter sets (excitation, 488 nm).

4.16. Biodistribution

A saline solution which contains the HPLC-purified ^{18}F-labled tracer (0.1 mL, 10% ethanol, 185 kBq) was injected via tail veins of the ICR mice (five weeks, male). The mice were then sacrificed by cervical fracture exactly at time points of 2, 10, 30 and 60 min. The samples of blood and interested organs were collected, weighed and counted separately in an automatic γ-counter (Wallac 1470 Wizard, USA). The final results were expressed in terms of the percentage of the injected dose per gram (% ID/g) of blood or organs with decay corrected.

4.17. Partition coefficient determination

The log *D* values of [^{18}F]**8** and [^{18}F]**9** were determined by measuring the distribution of the radiotracer between 1-octanol and PBS buffer (0.05 M) at pH = 7.4. The two phases were pre-saturated with each other. 1-octanol (3 mL) and PBS (3 mL) were pipetted into a 10 mL plastic centrifuge tube. 10 μL of HPLC-purified [^{18}F]**8** or [^{18}F]**9** (0.74 MBq) in ethanol was then added. The tube was vortexed for 5 min, followed by centrifugation for 15 min (3500 rpm, Anke TDL80-2B, China). Two samples removed from the *n*-octanol (50 μL) and water (500 μL) layers were separately measured by an automatic γ-counter (Wallac 1470 Wizard, USA). The distribution coefficient was determined by calculating the ratio of cpm/mL of 1-octanol layer to that of buffer layer and expressed as log *D*. Samples from the 1-octanol layer were re-distributed until consistent distribution coefficient values were obtained.

4.18. In vitro stability studies

The *in vitro* stability of [^{18}F]**8** and [^{18}F]**9** in saline and mouse plasma were examined by incubating 1.85 MBq purified [^{18}F]**8** or [^{18}F]**9** with 100 μL saline or mouse plasma at 37 °C for 2 min, 10 min, 30 min and 60 min. Proteins were precipitated by adding 200 μL acetonitrile. The supernatant was collected, after centrifugation at 5000 rpm for 5 min at 4 °C. A sample of approximately 0.1 mL of the supernatant solution was removed and subjected to HPLC for analysis.

Acknowledgments

This work was funded by National Natural Science Foundation of China (No: 21201019 and 81371593), Research Fund for the Doctoral Program of Higher Education of China (No: 20120003120013) and Fundamental Research Funds for the Central Universities (No: 2012LYB19). The authors present special thanks to Dr. Jin Liu (College of Life Science, Beijing Normal University) for assistance in the *in vitro* neuropathological staining, and declare no competing financial interest.

Appendix A. Supplementary data

Supplementary data related to this article can be found at http://dx.doi.org/10.1016/j.ejmech.2014.07.070.

References

[1] B.S. Shastry, Molecular genetics of familial Alzheimer disease, Am. J. Med. Sci. 315 (1998) 266–272.
[2] A. Wimo, B. Winblad, H. Aguero-Torres, E. von Strauss, The magnitude of dementia occurrence in the world, Alzheimer Dis. Assoc. Disord. 17 (2003) 63–67.
[3] E. Zamrini, S. De Santi, M. Tolar, Imaging is superior to cognitive testing for early diagnosis of Alzheimer's disease, Neurobiol. Aging 25 (2004) 685–691.
[4] D.J. Selkoe, Amyloid beta-protein and the genetics of Alzheimer's disease, J. Biol. Chem. 271 (1996) 18295–18298.
[5] B.A. Yankner, Mechanisms of neuronal degeneration in Alzheimer's disease, Neuron 16 (1996) 921–932.
[6] R.L. Nussbaum, C.E. Ellis, Alzheimer's disease and Parkinson's disease, N. Engl. J. Med. 348 (2003) 1356–1364.
[7] J. Hardy, D.J. Selkoe, The amyloid hypothesis of Alzheimer's disease: progress and problems on the road to therapeutics, Science 297 (2002) 353–356.
[8] D.J. Selkoe, Imaging Alzheimer's amyloid, Nat. Biotechnol. 18 (2000) 823–824.
[9] C.A. Mathis, Y. Wang, W.E. Klunk, Imaging beta-amyloid plaques and neurofibrillary tangles in the aging human brain, Curr. Pharm. Des. 10 (2004) 1469–1492.
[10] A. Nordberg, PET imaging of amyloid in Alzheimer's disease, Lancet Neurol. 3 (2004) 519–527.
[11] H. Benveniste, G. Einstein, K.R. Kim, C. Hulette, G.A. Johnson, Detection of neuritic plaques in Alzheimer's disease by magnetic resonance microscopy, PNAS 96 (1999) 14079–14084.
[12] J. Zhang, P. Yarowsky, M.N. Gordon, G. Di Carlo, S. Munireddy, P.C. van Zijl, S. Mori, Detection of amyloid plaques in mouse models of Alzheimer's disease by magnetic resonance imaging, Magn. Reson. Med. 51 (2004) 452–457.
[13] M. Higuchi, N. Iwata, Y. Matsuba, K. Sato, K. Sasamoto, T.C. Saido, ^{19}F and ^{1}H MRI detection of amyloid beta plaques in vivo, Nat. Neurosci. 8 (2005) 527–533.
[14] M. Ono, H. Saji, SPECT imaging agents for detecting cerebral beta-amyloid plaques, Int. J. Mol. Imaging 2011 (2011) 12, 543267.
[15] B.J. Bacskai, S.T. Kajdasz, R.H. Christie, C. Carter, D. Games, P. Seubert, D. Schenk, B.T. Hyman, Imaging of amyloid-beta deposits in brains of living mice permits direct observation of clearance of plaques with immunotherapy, Nat. Med. 7 (2001) 369–372.
[16] J. Skoch, A. Dunn, B.T. Hyman, B.J. Bacskai, Development of an optical approach for noninvasive imaging of Alzheimer's disease pathology, J. Biomed. Opt. 10 (2005) 11007.
[17] E.E. Nesterov, J. Skoch, B.T. Hyman, W.E. Klunk, B.J. Bacskai, T.M. Swager, In vivo optical imaging of amyloid aggregates in brain: design of fluorescent markers, Angew. Chem. Int. Ed. Engl. 44 (2005) 5452–5456.
[18] M. Hintersteiner, A. Enz, P. Frey, A.L. Jaton, W. Kinzy, R. Kneuer, U. Neumann, M. Rudin, M. Staufenbiel, M. Stoeckli, K.H. Wiederhold, H.U. Gremlich, In vivo detection of amyloid-beta deposits by near-infrared imaging using an oxazine-derivative probe, Nat. Biotechnol. 23 (2005) 577–583.
[19] C.A. Mathis, N.S. Mason, B.J. Lopresti, W.E. Klunk, Development of positron emission tomography beta-amyloid plaque imaging agents, Semin. Nucl. Med. 42 (2012) 423–432.
[20] S. Vallabhajosula, Positron emission tomography radiopharmaceuticals for imaging brain Beta-amyloid, Semin. Nucl. Med. 41 (2011) 283–299.
[21] C.A. Mathis, Y. Wang, D.P. Holt, G.F. Huang, M.L. Debnath, W.E. Klunk, Synthesis and evaluation of ^{11}C-labeled 6-substituted 2-arylbenzothiazoles as amyloid imaging agents, J. Med. Chem. 46 (2003) 2740–2754.
[22] W.E. Klunk, H. Engler, A. Nordberg, Y. Wang, G. Blomqvist, D.P. Holt, M. Bergstrom, I. Savitcheva, G.F. Huang, S. Estrada, B. Ausen, M.L. Debnath, J. Barletta, J.C. Price, J. Sandell, B.J. Lopresti, A. Wall, P. Koivisto, G. Antoni, C.A. Mathis, B. Langstrom, Imaging brain amyloid in Alzheimer's disease with Pittsburgh Compound-B, Ann. Neurol. 55 (2004) 306–319.
[23] M. Koole, D.M. Lewis, C. Buckley, N. Nelissen, M. Vandenbulcke, D.J. Brooks, R. Vandenberghe, K. Van Laere, Whole-body biodistribution and radiation dosimetry of ^{18}F-GE067: a radioligand for in vivo brain amyloid imaging, J. Nucl. Med. 50 (2009) 818–822.
[24] M. Ono, A. Wilson, J. Nobrega, D. Westaway, P. Verhoeff, Z.P. Zhuang, M.P. Kung, H.F. Kung, ^{11}C-labeled stilbene derivatives as Abeta-aggregate-specific PET imaging agents for Alzheimer's disease, Nucl. Med. Biol. 30 (2003) 565–571.
[25] N.P. Verhoeff, A.A. Wilson, S. Takeshita, L. Trop, D. Hussey, K. Singh, H.F. Kung, M.P. Kung, S. Houle, In-vivo imaging of Alzheimer disease beta-amyloid with [^{11}C]SB-13 PET, Am. J. Geriatr. Psychiatry 12 (2004) 584–595.
[26] C.C. Rowe, U. Ackerman, W. Browne, R. Mulligan, K.L. Pike, G. O'Keefe, H. Tochon-Danguy, G. Chan, S.U. Berlangieri, G. Jones, K.L. Dickinson-Rowe, H.P. Kung, W. Zhang, M.P. Kung, D. Skovronsky, T. Dyrks, G. Holl, S. Krause, M. Friebe, L. Lehman, S. Lindemann, L.M. Dinkelborg, C.L. Masters, V.L. Villemagne, Imaging of amyloid beta in Alzheimer's disease with ^{18}F-

BAY94-9172, a novel PET tracer: proof of mechanism, Lancet Neurol. 7 (2008) 129–135.
[27] S.R. Choi, G. Golding, Z. Zhuang, W. Zhang, N. Lim, F. Hefti, T.E. Benedum, M.R. Kilbourn, D. Skovronsky, H.F. Kung, Preclinical properties of ^{18}F-AV-45: a PET agent for Abeta plaques in the brain, J. Nucl. Med. 50 (2009) 1887–1894.
[28] H.F. Kung, S.R. Choi, W. Qu, W. Zhang, D. Skovronsky, ^{18}F stilbenes and styrylpyridines for PET imaging of A beta plaques in Alzheimer's disease: a miniperspective, J. Med. Chem. 53 (2010) 933–941.
[29] E.D. Agdeppa, V. Kepe, J. Liu, S. Flores-Torres, N. Satyamurthy, A. Petric, G.M. Cole, G.W. Small, S.C. Huang, J.R. Barrio, Binding characteristics of radiofluorinated 6-dialkylamino-2-naphthylethylidene derivatives as positron emission tomography imaging probes for beta-amyloid plaques in Alzheimer's disease, J. Neurosci. 21 (2001) RC189.
[30] K. Shoghi-Jadid, G.W. Small, E.D. Agdeppa, V. Kepe, L.M. Ercoli, P. Siddarth, S. Read, N. Satyamurthy, A. Petric, S.C. Huang, J.R. Barrio, Localization of neurofibrillary tangles and beta-amyloid plaques in the brains of living patients with Alzheimer disease, Am. J. Geriatr. Psychiatry 10 (2002) 24–35.
[31] E.D. Agdeppa, V. Kepe, J. Liu, G.W. Small, S.C. Huang, A. Petric, N. Satyamurthy, J.R. Barrio, 2-Dialkylamino-6-acylmalononitrile substituted naphthalenes (DDNP analogs): novel diagnostic and therapeutic tools in Alzheimer's disease, Mol. Imaging Biol. 5 (2003) 404–417.
[32] C.C. Rowe, V.L. Villemagne, Brain amyloid imaging, J. Nucl. Med. 52 (2011) 1733–1740.
[33] M. Cui, M. Ono, H. Kimura, B. Liu, H. Saji, Synthesis and structure-affinity relationships of novel dibenzylideneacetone derivatives as probes for beta-amyloid plaques, J. Med. Chem. 54 (2011) 2225–2240.
[34] L. Cai, R.B. Innis, V.W. Pike, Radioligand development for PET imaging of beta-amyloid (Abeta)–current status, Curr. Med. Chem. 14 (2007) 19–52.
[35] H. Toyama, D. Ye, M. Ichise, J.S. Liow, L. Cai, D. Jacobowitz, J.L. Musachio, J. Hong, M. Crescenzo, D. Tipre, J.Q. Lu, S. Zoghbi, D.C. Vines, J. Seidel, K. Katada, M.V. Green, V.W. Pike, R.M. Cohen, R.B. Innis, PET imaging of brain with the beta-amyloid probe, [^{11}C]6-OH-BTA-1, in a transgenic mouse model of Alzheimer's disease, Eur. J. Nucl. Med. Mol. Imaging 32 (2005) 593–600.
[36] M. Cui, X. Wang, P. Yu, J. Zhang, Z. Li, X. Zhang, Y. Yang, M. Ono, H. Jia, H. Saji, B. Liu, Synthesis and evaluation of novel ^{18}F labeled 2-pyridinylbenzoxazole and 2-pyridinylbenzothiazole derivatives as ligands for positron emission tomography (PET) imaging of beta-amyloid plaques, J. Med. Chem. 55 (2012) 9283–9296.
[37] Z.P. Zhuang, M.P. Kung, A. Wilson, C.W. Lee, K. Plossl, C. Hou, D.M. Holtzman, H.F. Kung, Structure-activity relationship of imidazo[1,2-a]pyridines as ligands for detecting beta-amyloid plaques in the brain, J. Med. Chem. 46 (2003) 237–243.